Published by Nigerian Society of Physical Sciences. Hosted by FLAYOO Publishing House LTD

Check for updates

Recent Advances in Natural Sciences

Journal Homepage: https://flayoophl.com/journals/index.php/rans

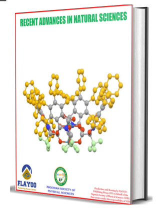

Coupled optical and electrical modeling of TiO_2 anti-reflective coatings for enhanced performance in GaAs thin-film solar cells

F. Aungwa[a,*], D. S. Igba[a], A. A. McAsule[a,b], M. B. Ochang[a], W. V. Zhiya[a], A. I. Tyom[a]

[a]*Department of Industrial Physics, Joseph Sarwuan Tarka University (University of Agriculture Makurdi), P.M.B. 2373, Makurdi, Benue State, Nigeria*
[b]*School of Physics, Universiti Sains Malaysia, 11800 USM, Pulau Penang, Malaysia*

ARTICLE INFO

Article history:
Received: 28 April 2026
Received in revised form: 11 July 2026
Accepted: 12 July 2026
Available online: 31 July 2026

Keywords: TiO_2 anti-reflective coating, GaAs thin-film solar cell, Optical–electrical modeling, Photovoltaic efficiency

DOI:10.61298/rans.2026.4.2.367

ABSTRACT

Optical reflection losses at the air–semiconductor interface limit the performance of gallium arsenide (GaAs) thin-film solar cells, whereas optical and electrical optimization are often considered separately. This study develops a coupled MATLAB-based optical–electrical simulation framework to evaluate the effect of titanium dioxide (TiO_2) anti-reflective coating (ARC) thickness on GaAs thin-film solar cells. The optical response was assessed from wavelength-dependent reflectance, transmittance, absorptance, and quantum efficiency, and electrical performance was evaluated from current density–voltage characteristics, short-circuit current density (J_{sc}), open-circuit voltage (V_{oc}), fill factor (FF), and power conversion efficiency (PCE). TiO_2 ARC thicknesses of 50, 75, and 100 nm were simulated under AM 1.5G illumination at 300 K. The 50 nm coating produced the lowest reflectance, highest absorptance, highest current density, and highest quantum efficiency across 300–900 nm. It also provided the best overall photovoltaic performance, with $J_{sc} \approx 34.7$ mA cm^{-2}, $V_{oc} \approx 0.839$ V, FF ≈ 0.842, and a maximum PCE of approximately 24.2%. Increasing the coating thickness to 75 and 100 nm reduced the PCE to approximately 22.95% and 21.85%, respectively. The results show that optimum photovoltaic efficiency requires a balanced combination of optical absorption, current generation, voltage, and FF. The coupled framework provides a computationally efficient tool for designing and optimizing ARCs for high-efficiency III–V photovoltaic devices.

1. INTRODUCTION

The growing use of renewable energy has prompted substantial research into solar photovoltaic (PV) technology. Solar energy is one of the most abundant and rapidly expanding renewable energy sources [1]. A PV cell converts incident solar energy into electricity through the photovoltaic effect. Solar cells are fabricated from several materials, including silicon, amorphous silicon (a-Si), gallium arsenide (GaAs), copper indium selenide (CIS), and copper indium gallium selenide (CIGS) [2, 3].

Silicon solar cells are widely used because silicon is abundant, inexpensive, and relatively benign. The limited efficiency of first-generation devices motivated the development of second-generation semiconductor thin-film technologies, including CIS, self-assembled monolayers (SAMs), and a-Si [4]. The per-

*Corresponding author Tel. No.: +234-703-068-2458.
e-mail: francisaungwa@gmail.com (F. Aungwa)

formance and stability limitations of earlier generations subsequently encouraged the development of third-generation PV technologies [5]. A major obstacle to thin-film solar-cell efficiency is optical loss caused by surface reflection, which prevents part of the incident sunlight from being absorbed by the active layer. This loss directly affects the power conversion efficiency (PCE), making it necessary to investigate methods for reducing reflection and enhancing light absorption.

Photoelectric conversion efficiency remains a central concern as solar-cell performance continues to improve [6]. Several processes influence efficiency under operating conditions. Reflection loss at the surface and heat generation by high-energy charge carriers in the short-wavelength region are two important mechanisms that reduce solar-cell performance [7]. An anti-reflective coating (ARC) is an effective method for reducing reflection loss and heat generation at the front surface of a solar cell [8].

Materials investigated for high-performance ARCs include silicon dioxide (SiO_2), magnesium fluoride (MgF_2), aluminum oxide (Al_2O_3), and titanium dioxide (TiO_2). TiO_2 is attractive because of its high refractive index (approximately 2.7), nontoxicity, abundance, low cost, low absorption in the visible range, and self-cleaning properties [9]. Destructive interference can reduce Fresnel reflection when light propagates between media with different refractive indices, such as an ARC and a solar-cell substrate. However, the effects of ARC thickness and temperature rise on solar-cell efficiency have not been investigated as extensively as their individual optical effects. Evaluating both the optical and electrical properties of coated solar cells is therefore important for developing practical ARCs with improved performance [10].

Leem *et al.* [11] reported that a 50-nm-thick nanostructured TiO_2 ARC reduced the reflectance of single-junction solar cells to 6.2% over the 350–900 nm wavelength range at incidence angles of 30–80°, compared with cells without an ARC. Hammad *et al.* [12] found that the maximum efficiency of clean and dusty silicon solar panels without an ARC decreased by 15% and 16%, respectively, as the temperature increased from 40 to 50 °C. Lorenzi *et al.* [7] conducted experimental and modeling studies of temperature-dependent power losses and showed that increasing temperature significantly reduced the open-circuit voltage.

Despite extensive studies of ARCs, most existing work focuses primarily on either optical optimization or electrical performance [13, 14]. In addition, many simulation approaches use complex multiphysics platforms, which can limit accessibility and computational efficiency [15, 16]. A simplified but accurate framework that directly couples optical absorption to electrical output is therefore needed for efficient prediction and optimization of photovoltaic performance [9, 17].

This study introduces a computationally efficient MATLAB-based framework that establishes a direct relationship between ARC-induced optical enhancement and electrical performance. Unlike approaches that treat these effects separately, the proposed method provides an integrated tool for predicting photovoltaic behavior and rapidly optimizing ARC thickness for high-efficiency solar cells. Theoretical analysis of ARCs is important for maximizing their performance in thin-film solar cells, and mathematical modeling and computational simulation provide useful information on how ARC characteristics affect solar-cell efficiency [13].

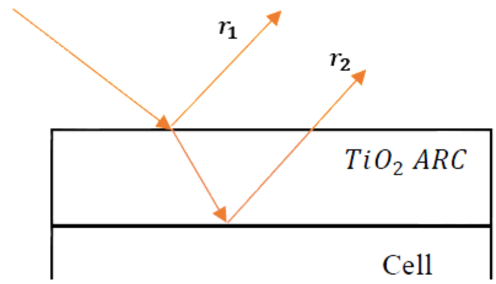

Figure 1. Interference of light through the coating and substrate layers [18].

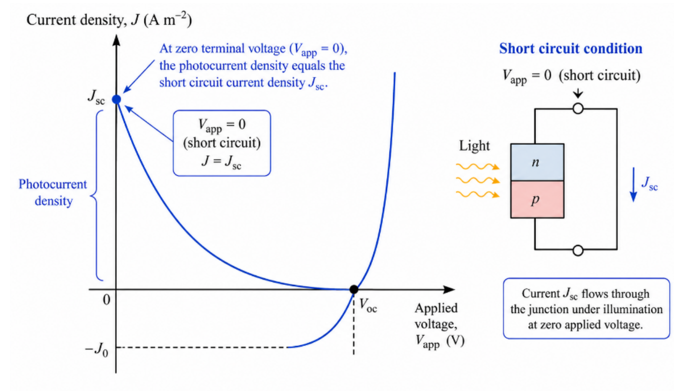

Figure 2. Current density–voltage characteristics of a photovoltaic junction under short-circuit conditions ($V_{app} = 0$, $J = J_{sc}$).

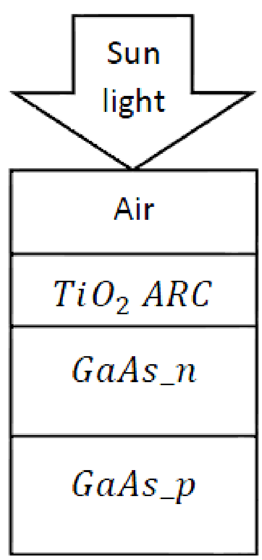

Figure 3. Schematic of a GaAs solar cell coated with a TiO_2 ARC [19].

2. METHODOLOGY AND THEORETICAL CONSIDERATIONS

The analysis combined optical and electrical theories. The optical component described the reflection of electromagnetic waves in the visible region, whereas the electrical component related the optical response to current density, open-circuit voltage, maximum power, and solar-cell efficiency.

Table 1. Simulation parameters [20].

Parameter	GaAs (*n*-type)	GaAs (*p*-type)
Relative permittivity	13.8	13.8
Band gap	1.4 eV	1.4 eV
Electron affinity	4.2 eV	4.2 eV
Effective density of states, N_c	1×10^{16} cm^{-3}	3×10^{18} cm^{-3}
Effective density of states, N_v	1×10^{16} cm^{-3}	3×10^{18} cm^{-3}
Electron mobility	1100 cm^2 V^{-1} s^{-1}	1100 cm^2 V^{-1} s^{-1}
Hole mobility	300 cm^2 V^{-1} s^{-1}	300 cm^2 V^{-1} s^{-1}
Electron lifetime	100 μs	100 μs
Hole lifetime	100 μs	100 μs
Temperature	300 K	300 K
Donor/acceptor concentration	9×10^{19} cm^{-3}	1×10^{21} cm^{-3}
Light intensity	0.1 W cm^{-2}	0.1 W cm^{-2}

2.1. CURRENT DENSITY–VOLTAGE CHARACTERIZATION AND THE INFLUENCE OF ANTI-REFLECTIVE COATINGS

The current–voltage characteristic of a photovoltaic cell is governed by the superposition principle, under which the total device current is the algebraic sum of the dark diode current and the light-generated current. Under dark conditions, a solar cell behaves as a rectifying diode. Under illumination, incident photons generate electron–hole pairs that add a photocurrent component to the net current and shift the current–voltage curve into the power-generating quadrant.

The total current I as a function of applied voltage V is described by the ideal diode equation under illumination [21]:

$$I = I_0\left[\exp\left(\frac{qV}{nkT}\right) - 1\right] - I_L, \tag{1}$$

where I_0 is the dark saturation current, q is the elementary charge (1.602×10^{-19} C), n is the diode ideality factor, k is the Boltzmann constant, T is the absolute temperature, and I_L is the light-generated current.

The ARC is important for maximizing I_L. By minimizing the reflection coefficient at the cell surface, the coating increases the photon flux entering the semiconductor absorber. In current–voltage characterization, an effective ARC produces a vertical shift in the curve, increasing the short-circuit current and, consequently, the PCE.

2.2. OPTICAL CHARACTERIZATION

An ARC minimizes optical reflection at the air–semiconductor interface by promoting destructive interference between light reflected from the air/ARC interface and light reflected from the ARC/substrate interface. For a single-layer ARC, the theoretical optimum refractive index is the geometric mean of the refractive indices of the incident medium and the substrate:

$$n_{ARC} = \sqrt{n_0 n_s}, \tag{2}$$

where n_0 is the refractive index of air and n_s is the refractive index of the GaAs substrate. Materials with the exact optimum refractive index are not always readily available [22]. Practical ARC design therefore requires selection of an appropriate material and optimization of its thickness to achieve the desired interference condition and minimize surface reflection.

For normal incidence, destructive interference is maximized when the optical thickness of the coating satisfies the quarter-wavelength condition:

$$d = \frac{\lambda}{4n_{ARC}}, \tag{3}$$

where d is the coating thickness, λ is the design wavelength, and n_{ARC} is the refractive index of the coating material. Under this condition, the reflected waves have a phase difference of 180°, resulting in destructive interference and reduced reflectance. Varying the coating thickness changes the optical path length and interference behavior but does not change the intrinsic refractive index of a homogeneous TiO_2 coating, which is determined by its composition and microstructure.

The optical phase difference associated with the coating thickness and refractive index can be modeled as

$$\theta = \frac{2\pi d n_{ARC}}{\lambda}. \tag{4}$$

Because coating thickness and optical path difference are directly proportional [23], experimental deposition remains challenging owing to surface roughness at the heterogeneous coating/substrate interface, as illustrated in Figure 1.

The resultant reflectivity at the coating/solar-cell interface can be represented by

$$R = |r_2| = \frac{r_1^2 + r_2^2 + 2r_1 r_2\cos(2\theta)}{1 + r_1^2 r_2^2 + 2r_1 r_2\cos(2\theta)}, \tag{5}$$

where r_1 and r_2 denote the reflection contributions from the coating and substrate interfaces, respectively.

2.3. ELECTRICAL CHARACTERIZATION

When photons are absorbed by a solar cell, they excite electrons from the valence band to the conduction band [24]. This process creates electron–hole pairs, and carrier motion in the depletion region produces an electric current under the junction electric field. The output current density can be calculated from the equivalent circuit of the single-diode model [25]:

$$J = J_{ph} - J_0\left[\exp\left(\frac{q(V + JR_s)}{nk_BT}\right) - 1\right] - \frac{V - R_sJ}{R_{sh}}, \tag{6}$$

where J is the output current density (mA cm^{-2}), J_0 is the diode saturation current density (mA cm^{-2}), J_{ph} is the photocurrent density (mA cm^{-2}), R_s is the series resistance (Ω), R_{sh} is the shunt resistance (Ω), k_B is the Boltzmann constant (1.38×10^{-23} J K^{-1}), q is the elementary charge, V is the terminal voltage, n is the diode ideality factor, and T is the cell temperature in kelvin.

At zero terminal voltage, the photocurrent density is equivalent to the short-circuit current density J_{sc}, which is the current density through the junction under illumination at zero applied voltage ($V_{app} = 0$), as illustrated in Figure 2 [25]. When the terminal current density is zero ($J = 0$), the open-circuit voltage is

$$V_{oc} = \frac{nk_BT}{q}\ln\left(\frac{J_{sc}}{J_0} + 1\right). \tag{7}$$

The maximum power output can be obtained from the current density–voltage curve or calculated as [26]

$$P_{out} = \mathrm{FF}\, J_{sc} V_{oc}, \tag{8}$$

where the dimensionless fill factor (FF) measures the deviation of the actual current density–voltage characteristic from the ideal characteristic. It is defined as

$$\mathrm{FF} = \frac{V_m I_m}{V_{oc} I_{sc}} = \frac{P_{max}}{V_{oc} I_{sc}}, \tag{9}$$

where V_m and I_m are the voltage and current at the maximum-power point, respectively.

The PCE compares the electrical power extracted from a solar cell with the incident solar power and is expressed as a percentage [27]:

$$\eta = \frac{P_{out}}{P_{in}} \times 100 = \frac{V_{oc} I_{sc} \mathrm{FF}}{P_{in}} \times 100. \tag{10}$$

Because V_{oc} is a function of temperature, temperature affects carrier generation and recombination at the junction and therefore the generated voltage. The temperature dependence of J_{sc}, V_{oc}, and efficiency should therefore be considered.

MATLAB was used to evaluate the reflection coefficient using Eqs. (4) and (5) and to calculate the electrical quantities using Eqs. (6)–(10), as applicable. The optical and electrical modules were coupled through a one-way sequential transfer in which the output of the optical module served as the input to the electrical module. The wavelength-dependent absorptance $A(\lambda)$ was calculated from the reflectance $R(\lambda)$ and transmittance $T(\lambda)$ as $A(\lambda) = 1 - R(\lambda) - T(\lambda)$. The absorptance profile was then used to calculate the spectrally resolved carrier-generation rate $G(\lambda)$ in the GaAs absorber:

$$G(\lambda) = \frac{\alpha(\lambda) I_0(\lambda) A(\lambda)}{h\nu}, \tag{11}$$

where $\alpha(\lambda)$ is the wavelength-dependent absorption coefficient of GaAs, $I_0(\lambda)$ is the AM 1.5G spectral irradiance, h is Planck's constant, and ν is the photon frequency. The total photocurrent density supplied to the single-diode model was obtained by integrating the carrier-generation rate over the simulated spectral range:

$$J_{ph} = q \int_{\lambda_{min}}^{\lambda_{max}} G(\lambda)\, d\lambda. \tag{12}$$

The resulting J_{ph} was substituted directly into Eq. (6) to solve for current density as a function of applied voltage. The resulting curve was used to derive V_{oc}, P_{out}, FF, and PCE using Eqs. (7)–(10). The coupling was executed for ARC thicknesses of 50, 75, and 100 nm. No feedback from the electrical module to the optical module was included, consistent with the assumption that carrier concentrations do not significantly perturb the optical-field distribution at the modeled device scale.

2.4. COMPUTATIONAL SIMULATION

MATLAB is a numerical computing and simulation environment for physics-based, engineering, and scientific applications. It supports the modeling and simulation of coupled phenomena in structural mechanics, optics, heat transfer, fluid dynamics, electromagnetics, and acoustics [28, 29]. In this work, the optical and electrical properties were coupled and simulated within MATLAB.

2.5. LAYER ARRANGEMENT AND INPUT PARAMETERS

The two-dimensional device structure was selected from previous literature [20]. As shown in Figure 3, the thickness of the *n*- and *p*-type GaAs solar-cell layers and the surrounding air region were set to 600 and 100 nm, respectively.

The MATLAB-based framework coupled optical and electrical models to evaluate device performance. The optical model required optical constants, illumination intensity, and reflector properties to calculate the total photogeneration rate. The electrical model required material and electrical parameters, including trap-assisted and Shockley–Read–Hall (SRH) recombination parameters. The principal simulation inputs are summarized in Table 1.

2.6. SIMULATION PROCEDURE

The optical and electrical performance of TiO_2 ARCs on GaAs thin-film solar cells was investigated using a MATLAB-based numerical framework. The material properties and structural parameters were defined according to Table 1. The inputs included refractive indices, band-gap energies, electron and hole mobilities, doping concentrations, operating temperature, and TiO_2 ARC thicknesses of 50, 75, and 100 nm.

Two coupled computational modules were implemented: an optical module for light absorption and photogeneration and an electrical module for carrier transport and recombination. The optical constants of the constituent layers and the incident illumination intensity were specified as inputs to the optical module, with boundary conditions at the air/ARC interface representing the top surface. For the electrical module, boundary conditions were applied at the back electrode to represent the bottom contact.

The wavelength-dependent reflectance, transmittance, and absorptance were evaluated using the interference-based formulations in Eqs. (2)–(5). Simulations were performed for ARC thicknesses of 50, 75, and 100 nm to assess the anti-reflection behavior and light-trapping capability of the TiO_2 coatings.

Electrical parameters, including photocurrent density, V_{oc}, FF, and PCE, were computed using Eqs. (6)–(10). All electrical simulations were performed under standard test conditions, corresponding to AM 1.5G solar illumination and an operating temperature of 300 K.

The optical and electrical models were coupled by using the absorptance profiles from the optical simulations to calculate wavelength-dependent carrier-generation rates in the semiconductor layer. Carrier-recombination processes and temperature-dependent effects were incorporated through the SRH recombination model. The framework was executed independently for each TiO_2 ARC thickness. Outputs included wavelength-resolved optical spectra, current density–voltage characteristics, and two-dimensional heat maps of reflectance, transmittance, and absorptance.

3. RESULTS AND DISCUSSION

The effect of TiO_2 ARC thickness on the optical and electrical performance of GaAs thin-film solar cells is presented in Figures 4–6. The results show a strong dependence of device performance on ARC thickness and a clear relationship between optical behavior and electrical output.

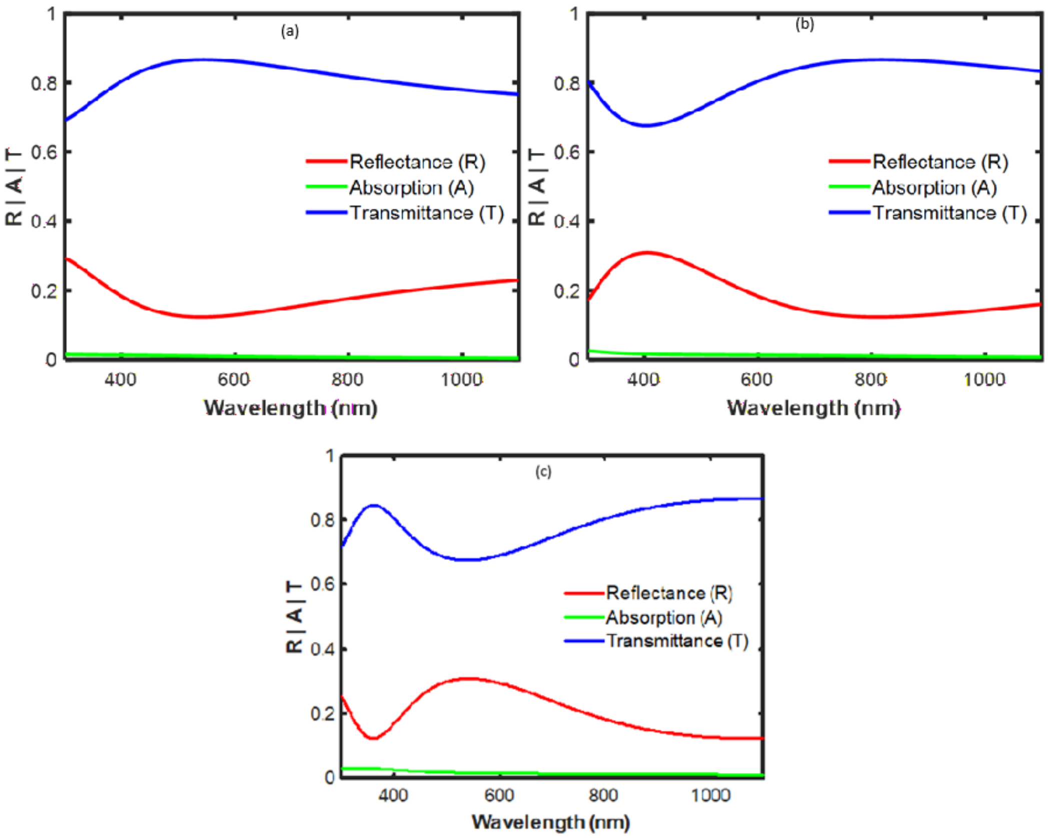

Figure 4. Optical properties of a TiO_2 ARC on a GaAs solar cell at thicknesses of (a) 50 nm, (b) 75 nm, and (c) 100 nm.

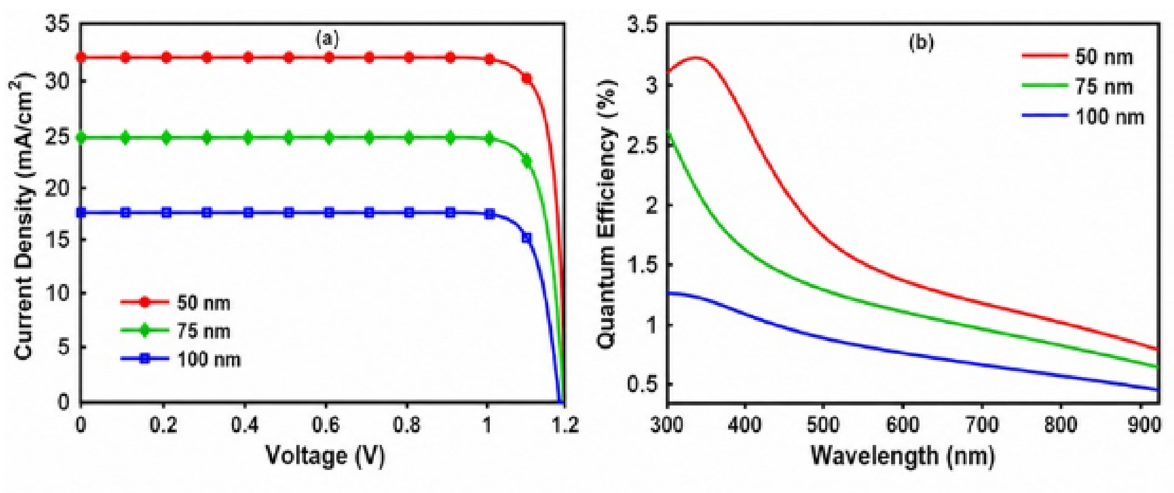

Figure 5. (a) Current density–voltage characteristics and (b) quantum-efficiency spectra of a GaAs solar cell with TiO_2 ARCs.

3.1. OPTICAL PROPERTIES

Figure 4 shows the reflectance, transmittance, and absorptance for TiO_2 ARC thicknesses of 50, 75, and 100 nm. As shown in Figure 4(a), the 50 nm coating exhibits the lowest reflectance and highest absorptance across the visible spectrum. This behavior indicates that the coating satisfies the quarter-wavelength condition in Eq. (3), thereby promoting destructive interference of the reflected waves and increasing light transmission into the GaAs absorber. Photon absorption is consequently maximized, consistent with Refs. [2, 9], which reported improved optical performance for optimized TiO_2 coatings.

As the thickness increases to 75 nm [Figure 4(b)], reflectance increases and absorptance decreases. This response indicates deviation from the optimum interference condition, such that the phase difference between the reflected waves no longer supports complete destructive interference. Similar behavior has been reported in Ref. [29], confirming that a non-optimum ARC thickness increases optical losses.

The trend is more pronounced at 100 nm [Figure 4(c)], where

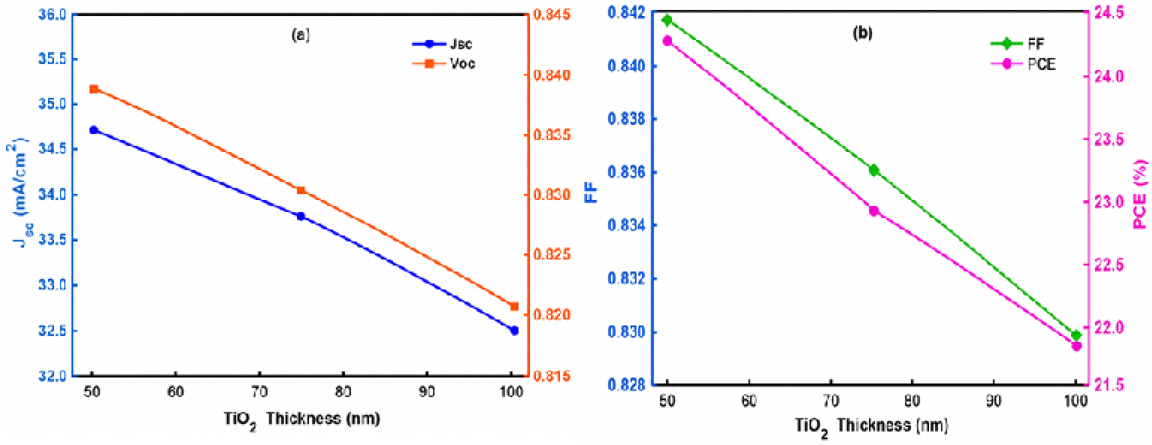

Figure 6. Dependence of (a) short-circuit current density and open-circuit voltage and (b) fill factor and power conversion efficiency on TiO_2 ARC thickness.

reflectance increases and absorptance is further reduced. The increased optical path length disrupts the interference condition, resulting in weaker anti-reflective performance. This observation is consistent with Ref. [13], which showed that excessive coating thickness can produce a phase mismatch and reduce light-trapping efficiency.

These results confirm that ARC thickness critically affects optical performance. Among the values studied, 50 nm provides the optimum condition for minimizing reflection and maximizing absorption. Deviations from this thickness introduce an optical mismatch and reduce the effectiveness of light trapping.

3.2. ELECTRICAL CHARACTERISTICS AND QUANTUM EFFICIENCY

Figure 5 presents the effect of TiO_2 ARC thickness on the electrical performance of the GaAs solar cell. Figure 5(a) indicates that J_{sc} decreases with increasing ARC thickness. Among the coatings investigated, the 50 nm TiO_2 layer produces the highest current density, followed by the 75 nm coating, whereas the 100 nm coating produces the lowest current density. The value of V_{oc} varies only slightly among the three thicknesses. The decrease in current density with increasing TiO_2 thickness is consistent with the reduced absorptance in Figure 4 as the coating departs from the quarter-wavelength condition, indicating that thickness-dependent optical losses directly limit carrier generation. This trend agrees with Refs. [16, 23], which discussed anti-reflective structures and photovoltaic parameter estimation.

A similar trend is described by the quantum-efficiency spectra in Figure 5(b). The 50 nm TiO_2 ARC exhibits the highest quantum efficiency over 300–900 nm, followed by the 75 nm coating, whereas the 100 nm coating exhibits the lowest quantum efficiency. The differences are most pronounced at short wavelengths (300–450 nm). Quantum efficiency gradually decreases with increasing wavelength for all thicknesses, but the stated performance ranking remains unchanged across the spectral range. The results indicate that departure from the optimum 50 nm thickness progressively reduces both the spectral response and carrier generation, consistent with the optical behavior in Figure 4 [13, 19].

3.3. THICKNESS DEPENDENCE OF PHOTOVOLTAIC PARAMETERS

Figure 6 illustrates the influence of TiO_2 ARC thickness on the photovoltaic performance of the GaAs solar cell. As shown in Figure 6(a), both J_{sc} and V_{oc} decrease as the coating thickness increases from 50 to 100 nm. The 50 nm ARC provides the highest J_{sc}, approximately 34.7 mA cm^{-2}, which decreases to 33.75 and 32.50 mA cm^{-2} for the 75 and 100 nm coatings, respectively. Similarly, V_{oc} decreases from approximately 0.839 V at 50 nm to 0.830 and 0.821 V at 75 and 100 nm, respectively. The reduction in J_{sc} indicates that increasing the TiO_2 coating thickness beyond 50 nm reduces the number of photogenerated carriers collected by the device. The corresponding decrease in V_{oc} reflects the lower carrier concentration associated with reduced photon absorption, as described by the single-diode model in Eq. (6). This behavior is consistent with Ref. [7], which reported that photovoltaic performance is strongly influenced by the device's optical-absorption characteristics.

Figure 6(b) shows a similar trend for FF and PCE, both of which decrease with increasing coating thickness. The 50 nm TiO_2 coating achieves the highest FF, approximately 0.842, and the maximum PCE, approximately 24.2%. At 75 nm, the FF decreases to approximately 0.836 and the PCE to 22.95%. At 100 nm, the FF and PCE decrease further to approximately 0.830 and 21.85%, respectively. The simultaneous reductions in J_{sc}, V_{oc}, and FF account for the decrease in conversion efficiency, demonstrating that departure from the optimum coating thickness adversely affects overall photovoltaic performance. These observations agree with Refs. [15, 19], which emphasized that precise optimization of ARC thickness is important for maximizing the efficiency of GaAs solar cells.

The maximum PCE of approximately 24.2% obtained with the 50 nm TiO_2 ARC compares favorably with values reported for similar GaAs/TiO_2 structures. Parajuli *et al.* [9] reported a PCE of 24.75% for a single-layer TiO_2 ARC with an optimum thickness of 62 nm, a difference of less than one percentage point from the present result. The difference in optimum thickness may arise from variations in the assumed refractive-index dispersion, device architecture, and simulation method. Bahrami *et al.* [30] reported a PCE of 16.97% for a double-layer Al_2O_3/TiO_2 ARC, highlighting the importance of coating design and thickness optimization. Although the efficiency obtained here is below the 29.1% record value reported for single-junction GaAs solar cells in Ref. [27], which employed advanced surface-passivation and photon-recycling techniques, the present results indicate that a carefully optimized single-layer TiO_2 ARC can substantially improve device performance within a simplified modeling framework.

The results in Figure 6 therefore show that photovoltaic performance is highly sensitive to TiO_2 ARC thickness. The 50 nm coating provides the most favorable balance among J_{sc}, V_{oc}, FF, and PCE. Together with the optical results in Figures 4 and 5, these findings confirm that careful thickness optimization is important for maximizing the performance of GaAs thin-film solar cells and reinforce the need for precise thickness control during fabrication.

4. CONCLUSION

This study theoretically examined the influence of TiO_2 ARC thickness on the optical and electrical performance of GaAs thin-film solar cells using a coupled MATLAB-based simulation. Optical performance was evaluated from reflectance, transmittance, absorptance, current density–voltage characteristics, and quantum efficiency, whereas electrical performance was assessed from J_{sc}, V_{oc}, FF, and PCE.

The results show that TiO_2 ARC thickness strongly influences both the optical and electrical behavior of the solar cell. The 50 nm coating produced the lowest reflectance, highest absorptance, highest current density, and highest quantum efficiency over 300–900 nm, indicating stronger light trapping and carrier generation than the thicker coatings. The same thickness provided the best overall device performance, yielding $J_{sc} \approx 34.7$ mA cm^{-2}, $V_{oc} \approx 0.839$ V, FF ≈ 0.842, and a maximum PCE of approximately 24.2%. Increasing the coating thickness to 75 and 100 nm gradually reduced the photovoltaic parameters, with the PCE decreasing to approximately 22.95% and 21.85%, respectively. Optimum photovoltaic performance therefore depends on an appropriate balance among optical absorption, current generation, voltage, and FF rather than on increasing the coating thickness.

The coupled framework establishes a direct relationship among TiO_2 ARC thickness, optical enhancement, and photovoltaic performance. Its predicted efficiency compares favorably with values reported for $GaAs/TiO_2$ solar cells, indicating its potential as a design and optimization tool for ARCs. The model is limited to homogeneous single-layer coatings under idealized conditions. Future work should therefore include experimental validation and extend the framework to multilayer, graded-index, or nanostructured ARCs, together with realistic material properties and fabrication effects.

DATA AVAILABILITY

Data will be made available upon reasonable request.

DECLARATION OF COMPETING INTEREST

The authors declare that they have no known competing financial interests or personal relationships that could have appeared to influence the work reported in this manuscript.

FUNDING

This research received no specific grant from any funding agency.

References

[1] M. Noman, S. Tu, S. Ahmad, F. U. Zafar, H. A. Khan, S. U. Rehman, M. Waqas, A. D. Khan & O. U. Rehman, "Assessing the reliability and degradation of 10–35 years field-aged PV modules", PLOS ONE **17** (2022) e0261066. https://doi.org/10.1371/journal.pone.0261066.

[2] B. P. Singh, S. K. Goyal & P. Kumar, "Solar PV cell materials and technologies: Analyzing the recent developments", Materials Today: Proceedings **43** (2021) 2843. https://doi.org/10.1016/j.matpr.2021.01.003.

[3] J. Pastuszak & P. Węgierek, "Photovoltaic cell generations and current research directions for their development", Materials **15** (2022) 5542. https://doi.org/10.3390/ma15165542.

[4] C. Ji, W. Liu, Y. Bao, X. Chen, G. Yang, B. Wei, F. Yang & X. Wang, "Recent applications of antireflection coatings in solar cells", Photonics **9** (2022) 906. https://doi.org/10.3390/photonics9120906.

[5] E. Mirabi, F. Akrami Abarghuie & R. Arazi, "Integration of buildings with third-generation photovoltaic solar cells: a review", Clean Energy **5** (2021) 505. https://doi.org/10.1093/ce/zkab031.

[6] J. Li, A. Aierken, Y. Liu, Y. Zhuang, X. Yang, J. H. Mo, R. K. Fan, Q. Y. Chen, S. Y. Zhang, Y. M. Huang & Q. Zhang, "A brief review of high efficiency III-V solar cells for space application", Front. Phys. **8** (2020) 631925. https://doi.org/10.3389/fphy.2020.631925.

[7] B. Lorenzi, M. Acciarri & D. Narducci, "Experimental determination of power losses and heat generation in solar cells for photovoltaic-thermal applications", Journal of Materials Engineering and Performance **27** (2018) 6291. https://doi.org/10.1007/s11665-018-3604-3.

[8] A. M. Mandong & A. Uzum, "Fresnel calculations of double/multi-layer antireflection coatings on silicon substrates", Research on Engineering Structures and Materials **7** (2021) 539. https://doi.org/10.17515/resm2020.241en1217.

[9] D. Parajuli, G. S. Gaudel, D. Kc, K. B. Khattri & W.-Y. Rho, "Simulation study of TiO_2 single layer anti-reflection coating for GaAs solar cell", AIP Advances **13** (2023) 085002. https://doi.org/10.1063/5.0153197.

[10] S. Zandi, P. Saxena, M. Razaghi & N. E. Gorji, "Simulation of CZTSSe thin-film solar cells in COMSOL: Three-dimensional optical, electrical, and thermal models", IEEE Journal of Photovoltaics **10** (2020) 1503. https://doi.org/10.1109/JPHOTOV.2020.2999881.

[11] J. W. Leem, J. S. Yu, D.-H. Jun, J. Heo & W.-K. Park, "Efficiency improvement of III–V GaAs solar cells using biomimetic TiO_2 subwavelength structures with wide-angle and broadband antireflection properties", Solar Energy Materials and Solar Cells **127** (2014) 43. https://doi.org/10.1016/j.solmat.2014.03.041.

[12] B. Hammad, M. Al-Abed, A. Al-Ghandoor, A. Al-Sardeah & A. Al-Bashir, "Modeling and analysis of dust and temperature effects on photovoltaic systems' performance and optimal cleaning frequency", Renewable and Sustainable Energy Reviews **82** (2018) 2218. https://doi.org/10.1016/j.rser.2017.08.070.

[13] L. Tian, L. Li & M. Wu, "Fabrication and characterisation of TiO_2 antireflection coatings with gradient index", Micro & Nano Letters **12** (2017) 849. https://doi.org/10.1049/mnl.2017.0408.

[14] A. S. Sarkin, N. Ekren & S. Saglam, "A review of anti-reflection and self-cleaning coatings on photovoltaic panels", Solar Energy **199** (2020) 63. https://doi.org/10.1016/j.solener.2020.01.084.

[15] S. D. Muhammad & M. H. Ali, "Evaluation of the effectiveness of TiO_2 antireflection coating for solar cell", Dutse Journal of Pure and Applied Sciences **10** (2024) 349. https://doi.org/10.4314/dujopas.v10i4a.32.

[16] A. K. Tenwar, S. Singh, I. Mal & D. P. Samajdar, "Anti-reflective nanostructures for efficiency improvement of GaAs-based solar cells", Materials Today: Proceedings **58** (2022) 682. https://doi.org/10.1016/j.matpr.2022.02.163.

[17] N. I. I. Mohd Jamaluddin, M. Z. Mohd Yusoff, M. F. Malek, R. G. Artes Jr. & J. S. Sala, "Simulation of a silicon solar cell using triple-layer antireflection coatings (ARC)", Key Engineering Materials **994** (2024) 61. https://doi.org/10.4028/p-6Rxxkp.

[18] H. Liu, J. Peng, W. Liu, Y. Wang, J. Wu, G. Zhang, X. Wang & Y. Yan, "Strong interference-based ultrathin conductive anti-reflection coating on metal substrates for optoelectronics", NPG Asia Materials **10** (2018) 309. https://doi.org/10.1038/s41427-018-0011-z.

[19] A. Abu-Shamleh, H. Alzubi & A. Alajlouni, "Optimization of antireflec-

tive coatings with nanostructured TiO_2 for GaAs solar cells'', Photonics and Nanostructures–Fundamentals and Applications **43** (2021) 100862. https://doi.org/10.1016/j.photonics.2020.100862.

[20] Y. He, Y. Tao, Z. Liu & Q. Huang, ''Design and optimization of nanostructure antireflection film for thin GaAs solar cells based on the photoelectrical coupling model'', Applied Energy **364** (2024) 123184. https://doi.org/10.1016/j.apenergy.2024.123184.

[21] S. Kim, V. Q. Hoang & C. W. Bark, ''Silicon-based technologies for flexible photovoltaic devices: From basic mechanism to manufacturing technologies'', Nanomaterials **11** (2021) 2944. https://doi.org/10.3390/nano11112944.

[22] Y. Zeng, A. Gentle, R. Webster, Z. Yang, Z. Zhou, N. Song, M. Keevers, M. Green & J. Y. Jiang, ''Revisiting photovoltaic module antireflection coatings: A novel, dense sol–gel design to address long-standing durability limitations'', Progress in Photovoltaics: Research and Applications **33** (2025) 1400. https://doi.org/10.1002/pip.3877.

[23] N. Gomidze, L. Kalandadze, O. Nakashide, I. Jabnidze, M. Khajishvili & J. Shainidze, ''Toward sustainable solar energy: analyzing key parameters in photovoltaic systems'', AIP Adv. **14** (2024) 110701. https://doi.org/10.1063/5.0243711.

[24] A. Martí, E. Antolín, C. R. Stanley, C. D. Farmer, N. López, P. Díaz, E. Cánovas, P. G. Linares & A. Luque, ''Production of photocurrent due to intermediate-to-conduction-band transitions: A demonstration of a key operating principle of the intermediate-band solar cell'', Physical Review Letters **97** (2006) 247701. https://doi.org/10.1103/PhysRevLett.97.247701.

[25] F. Aungwa, K. Ogunmoye, D. S. Igba, P. R. Jubu, A. A. Oche, E. Danladi, N. F. Gesa, A. T. Adepoju, E. J. Adoyi & M. B. Ochang, ''Optical thickness of dielectric layer in solar cell design for improved efficiency: A theoretical insight'', Physics Access **5** (2025) 67. https://doi.org/10.47514/phyaccess.2025.5.1.007.

[26] M. A. Green, ''Accurate expressions for solar cell fill factors including series and shunt resistances'', Applied Physics Letters **108** (2016) 081111. https://doi.org/10.1063/1.4942660.

[27] M. A. Green, E. D. Dunlop, D. H. Levi, J. Hohl-Ebinger, M. Yoshita & A. W. Y. Ho-Baillie, ''Solar cell efficiency tables (version 54)'', Progress in Photovoltaics: Research and Applications **27** (2019) 565. https://doi.org/10.1002/pip.3171.

[28] S. J. Yaqoob, A. L. Saleh, S. Motahhir, E. B. Agyekum, A. Nayyar & B. Qureshi, ''Comparative study with practical validation of photovoltaic monocrystalline module for single and double diode models'', Scientific Reports **11** (2021) 19153. https://doi.org/10.1038/s41598-021-98593-6.

[29] A. S. M. Mohsin, S. Mondal, M. Mobashera, A. Malik, M. Islam & M. Rubaiat, ''Efficiency improvement of thin film solar cell using silver pyramids array and antireflective layer'', Heliyon **9** (2023) e16749. https://doi.org/10.1016/j.heliyon.2023.e16749.

[30] A. Bahrami, S. Mohammadnejad, N. J. Abkenar & S. Soleimaninezhad, ''Optimized single- and double-layer antireflection coatings for GaAs solar cells'', International Journal of Renewable Energy Research **3** (2013) 79. Available online: https://dergipark.org.tr/en/pub/ijrer/issue/16080/168273.